Structural Insights into the Forward and Reverse Enzymatic Reactions in Human Adenine Phosphoribosyltransferase

Jessica Huyet, Mohammad Ozeir, Marie-Claude Burgevin, Anne Olivier-Bandini, Franck Auge, Benoît Pinson, Françoise Chesney, Jean-Marc Remy, Abdul Rauf Siddiqi, Roland Lupoli, et al.

Article

Cell Chemical Biology

Structural Insights into the Forward and Reverse Enzymatic Reactions in Human Adenine Phosphoribosyltransferase

Graphical Abstract

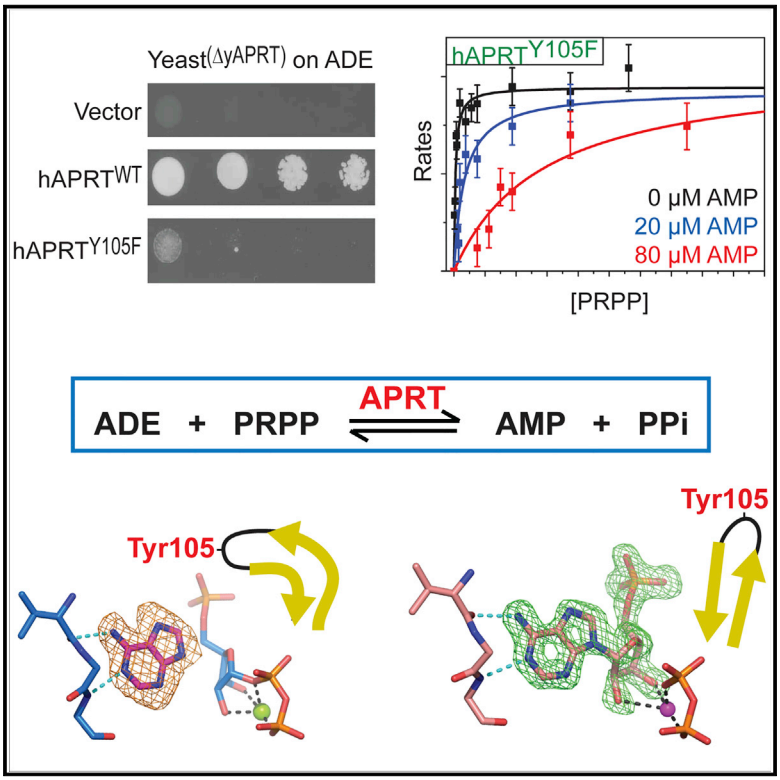

Authors

Jessica Huyet, Mohammad Ozeir, Marie-Claude Burgevin, ..., Anne Olivier-Bandini, Franck Augé, Pierre Nioche

Correspondence

franck.auge@sanofi.com (F.A.), pierre.nioche@gmail.com (P.N.)

In Brief

APRT is a key enzyme in the purine salvage pathway in prokaryotes and eukaryotes. Huyet et al., by using *in vitro*, cellular, and *in crystallo* enzymatic analyses, reveal that a hydroxyl group in a conserved tyrosine controls the protein dynamics and the catalytic efficiencies of the forward and reverse reactions.

Highlights

- Human APRT catalyzes the transformation of adenine into AMP and vice versa
- Complexes with substrates in both directions of the reaction highlight key residues
- The catalytic flexible loop dynamic is revealed by an *in crystallo* activity
- Tyr105 is essential for cell growth by facilitating the forward reaction

Huyet et al., 2018, Cell Chemical Biology *25*, 666–676
June 21, 2018
https://doi.org/10.1016/j.chembiol.2018.02.011

CellPress

CellPress

Cell Chemical Biology
Article

Structural Insights into the Forward and Reverse Enzymatic Reactions in Human Adenine Phosphoribosyltransferase

Jessica Huyet,[1,2,8] Mohammad Ozeir,[1,2,8] Marie-Claude Burgevin,[4] Benoît Pinson,[5] Françoise Chesney,[4] Jean-Marc Remy,[4] Abdul Rauf Siddiqi,[6] Roland Lupoli,[1,2,3] Gregory Pinon,[1,2,3] Christelle Saint-Marc,[5] Jean-Francois Gibert,[4] Renaud Morales,[4] Irène Ceballos-Picot,[7] Robert Barouki,[1,2,7] Bertrand Daignan-Fornier,[5] Anne Olivier-Bandini,[4] Franck Augé,[4,*] and Pierre Nioche[1,2,3,9,*]

[1]Université Paris Descartes, Sorbonne Paris Cité, UFR des Sciences Fondamentales et Biomédicales, UMR-S 1124, Centre Interdisciplinaire Chimie Biologie-Paris, 45, rue des Saints Pères, Paris 75006, France
[2]INSERM, UMR-S 1124, Paris 75006, France
[3]Université Paris Descartes, Structural and Molecular Analysis Platform, Paris 75006, France
[4]Sanofi R&D, Translational Science Unit, Chilly-Mazarin 91385, France
[5]Université de Bordeaux, Institut de Biochimie et Génétique Cellulaires, CNRS UMR 5095, Bordeaux Cedex 33077, France
[6]Department of Biosciences, COMSATS Institute of Information Technology, Islamabad, Pakistan
[7]Laboratoire de Biochimie Métabolomique et Protéomique, Hôpital Necker-Enfants Malades, Assistance Publique-Hôpitaux de Paris, Faculté de Médecine Paris Descartes, Paris 75015, France
[8]These authors contributed equally
[9]Lead Contact
*Correspondence: franck.auge@sanofi.com (F.A.), pierre.nioche@gmail.com (P.N.)
https://doi.org/10.1016/j.chembiol.2018.02.011

SUMMARY

Phosphoribosyltransferases catalyze the displacement of a PRPP α-1′-pyrophosphate to a nitrogen-containing nucleobase. How they control the balance of substrates/products binding and activities is poorly understood. Here, we investigated the human adenine phosphoribosyltransferase (hAPRT) that produces AMP in the purine salvage pathway. We show that a single oxygen atom from the Tyr105 side chain is responsible for selecting the active conformation of the 12 amino acid long catalytic loop. Using *in vitro*, cellular, and *in crystallo* approaches, we demonstrated that Tyr105 is key for the fine-tuning of the kinetic activity efficiencies of the forward and reverse reactions. Together, our results reveal an evolutionary pressure on the strictly conserved Tyr105 and on the dynamic motion of the flexible loop in phosphoribosyltransferases that is essential for purine biosynthesis in cells. These data also provide the framework for designing novel adenine derivatives that could modulate, through hAPRT, diseases-involved cellular pathways.

INTRODUCTION

Purine metabolism plays an important role in nucleic acid synthesis, energy-dependent reactions, and cellular signaling. This process synthesizes adenosine (AMP), guanosine (GMP), inosine (IMP), and xanthosine (XMP) nucleoside monophosphates either *de novo* or through a salvage pathway (Nyhan, 2005a; Zrenner et al., 2006). The recycling of purines is particularly important during periods of rapid growth, such as embryogenesis or tumor proliferation (Pillwein et al., 1990; Weber et al., 1987). Furthermore, the salvage pathway produces 90% of the cellular nucleotide pool overall, with purines coming from either nutrients or nucleotide catabolism via DNA and RNA degradation (Terkeltaub, 2012). Defects in purine homeostasis can lead to severe disorders, such as cancer, gout, anemia, urolithiasis, dystonia, intellectual disability, and immunodeficiency (Ceballos-Picot and Jinnah, 2016; Nyhan, 2005a, 2005b; de Vries and Sperling, 1977).

The regulation of purine metabolism is controlled by a number of key enzymes (Ceballos-Picot et al., 2015; Terkeltaub, 2012). One such enzyme in the salvage pathway is the adenine phosphoribosyltransferase (APRT, EC 2.4.2.7). Deficiencies in this enzyme lead to 2,8-dihydroxyadenine urolithiasis, and renal and allograft failures (Bollee et al., 2010; Ceballos-Picot et al., 2014; Zaidan et al., 2014). This enzyme with reversible activities has an ordered sequential bibi reaction mechanism (Bashor et al., 2002; Yuan et al., 1992). In the forward reaction, APRT synthesizes AMP and inorganic pyrophosphate (PPi) from adenine (ADE) and α-D-5-phosphoribosyl-1-pyrophosphate (PRPP) (Figure 1), using a divalent magnesium ion for catalysis. This is the favored reaction with a K_{eq} of around 10^5 for purified APRT from *Giardia lamblia*, as estimated by Haldane's representation (Sarver and Wang, 2002). In human cells, intracellular concentrations of adenine and AMP have been determined to be 1 μM and 200 μM, respectively (Curto et al., 1997). The concentration of PRPP and PPi, the other human APRT (hAPRT) substrates, are estimated to be 10 μM and 90 μM, respectively (Heinonen, 2001). The corresponding apparent K_Ms of hAPRT with ADE, PRPP, AMP, and PPi are of the order of 4 μM, 9 μM, 8 μM, and ~100 μM, respectively (Murray, 1967; Silva et al., 2004). In the forward reaction, ADE binds after PRPP, while in the reverse

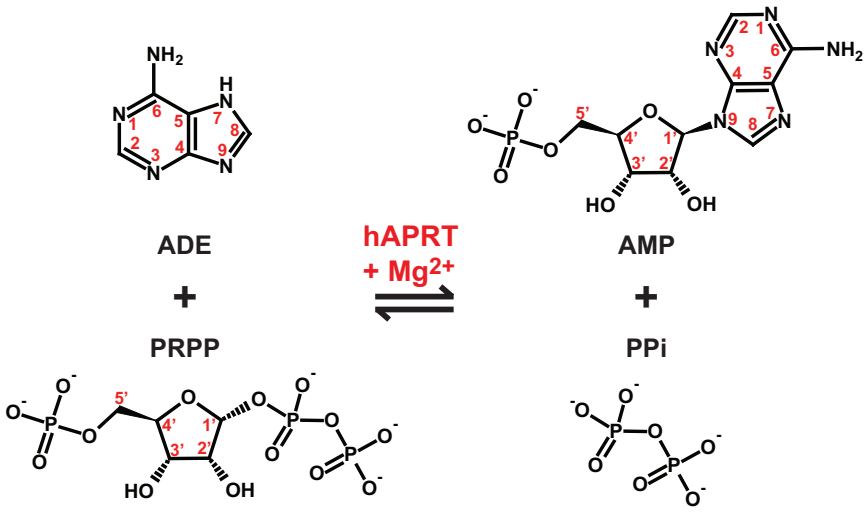

Figure 1. Chemical Structures of the hAPRT Substrates (ADE, AMP, PRPP, and PPi) for Both the Forward and Reverse Enzymatic Reactions

Atom numbering is indicated in red. See also Scheme S1.

reaction, AMP binds prior to PPi (Scheme S1) (Bashor et al., 2002). PRPP and AMP thus compete for the same site where the latter also acts as a competitive inhibitor of the forward reaction with a Ki value of 10.5 μM (Murray, 1967).

APRT refers to the type I phosphoribosyltransferase (PRT) family, which belongs to the large glycosyltransferase family (EC 2.4.). PRT structures are characterized by a Rossmann fold composed of a common core region formed by five central parallel beta strands flanked on each side by several alpha helices. The active site of APRT consists of a 13-amino-acid-long PRPP-binding motif, starting from Val123 in hAPRT, with a conserved A^{131}TGGS/T core sequence which serves to anchor the 5′ monophosphate group of either PRPP or ribonucleotides (Kabsch and Sander, 1983; Phillips et al., 1999; Sievers et al., 2011) (Figure S1A). It also contains two adjacent aspartates (Asp127 and Asp128 in hAPRT), two arginines (Arg67 and Arg87), and a specific cis-peptide bond, between Asp65 and Ser66, which hold together the 2′ and 3′-OH of the ribose and the pyrophosphate moiety of PRPP. The enzyme is a 180-amino-acid-long parallel homodimer. The two active sites are in proximity and interact via Arg87 from the opposite monomer. A hood region (amino acids 14 to 28) confers substrate selectivity, and a flexible loop (amino acids 99 to 110) usually closes over the binding site (Figure S1) (Eads et al., 1994; Schumacher et al., 1996; Shi et al., 1999). In 2008, the structures of hAPRT in the substrate-free form, as well as in the ADE-PRPP and AMP complexes were elucidated (Silva et al., 2008, 2004). These structures exhibited the expected fold of the type I PRT family. However, in the ADE-PRPP-Mg^{2+} complex (PDB: 1ZN7), the flexible loop was found in an unusual conformation with the conserved glutamate 104 oriented away from the adenine moiety (Silva et al., 2008). This observation contrasts with previously published structures of APRT enzyme from several other organisms (Phillips et al., 1999; Shi et al., 2002) that show the equivalent glutamate in hydrogen bonding distance to the ADE N7 position. Such discrepancies could relate to the fact that both the adenine and PRPP moieties are poorly defined in the electron density map (Figure S2) due to low occupancy of these substrates within the crystals together with the hydrolysis of PRPP leading to a non-catalytically active conformation of the enzyme (Deller and Rupp, 2015). More detailed structural parameters for hAPRT are therefore required to better understand how the adenine and PRPP substrates interact with and are processed by the enzyme.

Here, we report structural and biochemical studies with wild-type hAPRT, along with comparative results obtained with the hAPRT variant Tyr105Phe of the flexible loop. We present crystal structures of wild-type hAPRT in complex with PRPP-Mg^{2+}, ADE-PRPP-Mg^{2+}, and AMP. We also describe three structures of the Tyr105Phe hAPRT variant in complex with ADE, PRPP and Mg^{2+}, which were obtained during the enzymatic reaction time course. These structures allowed us to demonstrate a loop motion-dependent catalytic activity during a conversion, within crystals, of adenine and PRPP into AMP and PPi. Moreover, we show that Tyr105 is essential for driving hAPRT into a catalytically competent conformation, allowing the product to form and preventing the inhibition by AMP. This findings are relevant for other phosphoribosyltransferase enzymes and may pave the way for novel therapeutic applications against parasites (Berens et al., 1995; Gutierrez et al., 2009) or purine-associated diseases (Bollee et al., 2012; Hertz et al., 2013; Ceballos-Picot and Jinnah, 2016; Khan et al., 2006). Our results are particularly important in the context of Parkinson disease, for which the Parkinson-disease-related kinase (PINK1) is implicated in dopaminergic neuron degeneration and is regulated by adenine derivatives processed by hAPRT (Hertz et al., 2013). Our data, therefore, offers potential new applications against neurodegenerative diseases in humans.

RESULTS

Structures of PRPP-Mg^{2+}-, ADE-PRPP-Mg^{2+}-, and AMP-hAPRT

We first investigated the ligand-binding properties of hAPRT using differential scanning fluorimetry (DSF). Compared with the substrate-free form, we found that the unfolding temperature of the PRPP-bound enzyme was increased by 30°C, which suggests that PRPP protects the enzyme from thermodenaturation (Table S1). Stabilizing effects of such magnitude are rarely seen in proteins (Niesen et al., 2007). We also evidenced that adding adenine (ADE) to the PRPP-bound enzyme did not stabilize the complex further, since similar unfolding temperatures (Tm) were observed. Finally, adding AMP to the substrate-free protein stabilized the enzyme by only 10°C. To further study the role exerted by PRPP on hAPRT stability, we compared the crystal structure of PRPP-Mg^{2+}-bound hAPRT to the ADE-PRPP-Mg^{2+} and AMP complex structures. hAPRT with freshly prepared PRPP were co-crystallized using slightly modified

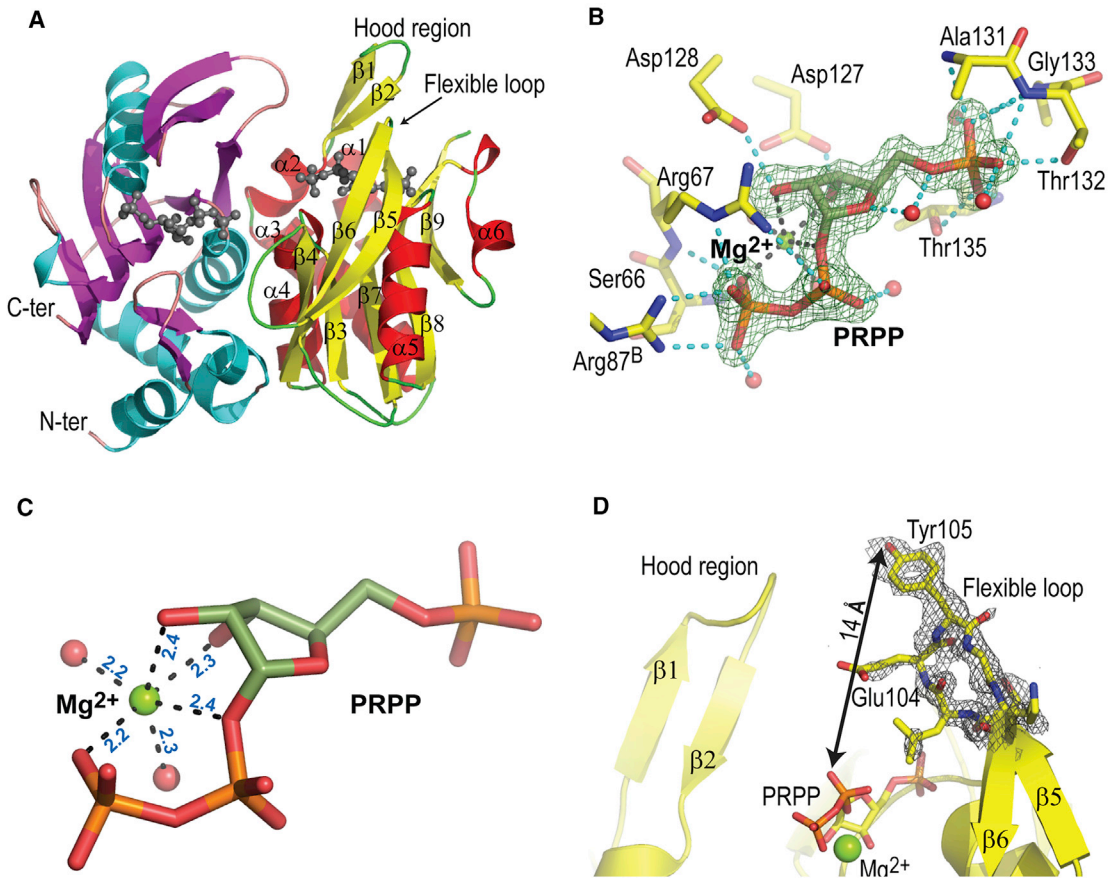

Figure 2. Structure of PRPP-Mg^{2+}-Bound $hAPRT^{wt}$

(A) Overall structure of the human APRT homodimer showing two PRPP molecules (gray ball-stick), the hood region, and the flexible loop.

(B) $F_o - F_c$ omit electron density map for PRPP contoured at 3σ. Arg87 comes from the other subunit (molecule B).

(C) Octahedral coordination of the magnesium ion. Coordinating distances in Å are indicated in blue.

(D) Detail of the flexible loop in the open conformation of the PRPP-bound $hAPRT^{wt}$ structure showing the Tyr105 away from the active site. The $F_o - F_c$ omit electron density map for residue 102 to 107 is contoured at 3σ. All the figures were generated with PyMOL (http://www.pymol.org/). The hydrogen bond distances are indicated in Å and represented with dashed cyan lines and Mg^{2+} coordinating interactions are marked as black dashed lines throughout.

See also Figures S1, S4, and Tables S1 and S2.

crystallization conditions from Silva et al. (2008). The first structure that only contains PRPP bound to a eukaryotic type I PRT enzyme was obtained with crystals diffracting to 1.45 Å resolution in the P1 space group with a single homodimer per asymmetric unit (Figure 2A, Table S2). One PRPP substrate was bound to each molecule of the asymmetric unit. The $F_o - F_c$ omit density showed full occupancy of the site, where PRPP interacts with all the components of its binding motif (Ala131, Thr132, Gly133, Thr135, Asp127, and Asp128) demonstrating a non-hydrolyzed substrate (Figure 2B). The pyrophosphate moiety was stabilized by Ser66, Arg67, and Arg87 from the second subunit of hAPRT and the magnesium ion. The latter exhibited a canonic octahedral configuration, coordinating two water molecules and four oxygen atoms of the PRPP substrate with bond distances varying between 2.2 and 2.4 Å (Figure 2C). We observed a well-defined flexible loop that exhibited an open conformation, with the conserved Glu104 and Tyr105 oriented away from the active site, which terminated with a PRPP-Tyr105 hydroxyl distance of over 14 Å (Figure 2D).

To investigate the role of the hAPRT flexible loop, we co-crystallized the enzyme with ADE, Mg^{2+}, and freshly prepared PRPP. Fourteen days after crystallization, the crystals were harvested and the structure determined. We found that both the PRPP and ADE substrates were well ordered in all four subunits of the asymmetric unit (Figures 3A, S3, and Table S2). The structure of the PRPP substrate was superimposable with our PRPP-bound hAPRT molecule (Figure 3A), which indicates that ADE binding does not promote modifications in the PRPP-binding site. ADE was found to interact with Val25, Arg27, Arg67, and Glu104 through hydrogen bonds. On each side of the purine plane, ADE maintained close van der Waals contacts with Phe26, Tyr105, Leu129, and Leu159. In addition, the conserved Tyr105 interacts through two hydrogen bonds with Arg67 and the 1′-pyrophosphate moiety. Tyr105 also positions its side chain above ADE to prevent the solvent from accessing both the N9 and C1′ atoms where the chemical reaction takes place. These contacts brought together both the flexible loop and the hood region to cover the active site. The organization of these

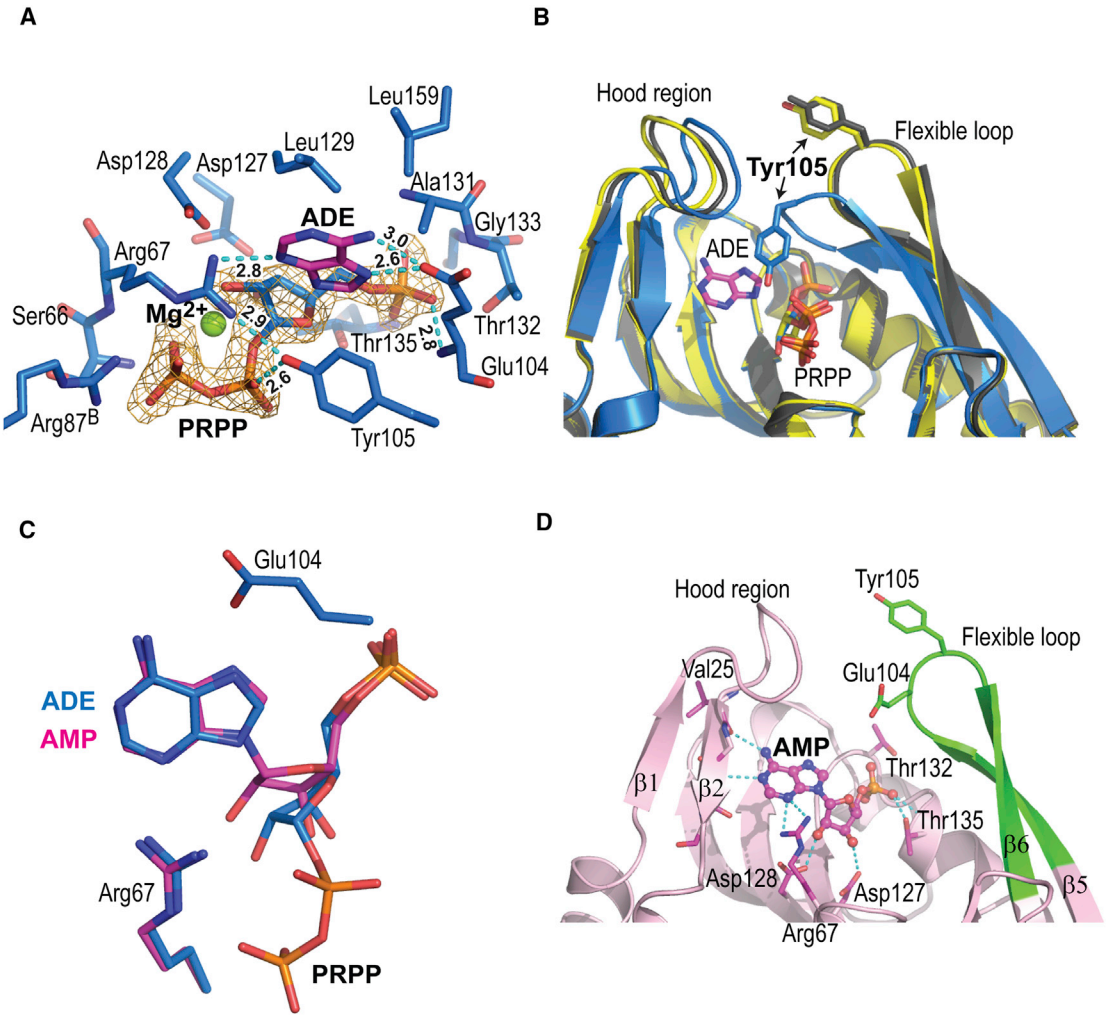

Figure 3. Structures of the ADE-PRPP-Mg^{2+}- and AMP-Bound $hAPRT^{wt}$

(A) $F_o - F_c$ omit electron density map for PRPP contoured at 3σ.

(B) Superimposition of our PRPP-Mg^{2+}- (yellow) and ADE-PRPP-Mg^{2+}- (blue) $hAPRT^{wt}$ complexes onto the previously determined ADE-PRPP-Mg^{2+}-$hAPRT^{wt}$ structure (gray) (PDB: 1ZN7).

(C) Close-up view of the ligands after superimposition of the ADE-PRPP-Mg^{2+}- onto AMP-$hAPRT^{wt}$ structures. ADE and PRPP are in blue, AMP in magenta, along with the corresponding amino acids in the active site.

(D) Structure of the AMP-$hAPRT^{wt}$ complex showing the flexible loop in an open conformation as in the PRPP-Mg^{2+}-$hAPRT^{wt}$ structure.

See also Figures S1–S5 and Tables S1 and S2.

two adaptable regions was different in our PRPP-bound structure compared with the previously reported ADE-PRPP-hAPRT structure (Silva et al., 2008). This was illustrated by the displacements of 2.9 Å of the alpha carbon of Val22 from the hood and of 6.3 Å of the alpha carbon of Tyr105 from the flexible loop in the ADE-PRPP-Mg^{2+}-hAPRT structure versus the PRPP-Mg^{2+}-bound structure (Figures 3B and S3E).

We could monitor product formation in solution using buffer conditions identical to those used for crystallization, but the k_{cat} measured in our assay decreased by 15-fold compared with a regular buffer (Tris, $MgCl_2$) (Table 1; Figures S4A and S4B). However, as clearly indicated by the structure, the forward enzymatic reaction did not occur in the crystals, even after 14 days, as the two substrates (ADE and PRPP) and the magnesium ion remain stable in the active site with full occupancy. Therefore, we never visualized *in crystallo* enzymatic activity in ADE-PRPP-Mg^{2+}-$hAPRT^{wt}$ crystals despite a close distance of 3.2 Å between N9 from ADE and C1′ from PRPP, which is a suitable distance to initiate the reaction.

Because AMP competes with PRPP for hAPRT activity, we next compared our PRPP structure to an AMP-bound structure. We diffused AMP molecules into substrate-free crystals and resolved the structure to 1.5 Å resolution. The electron density map in the active site was readily attributable to AMP (Figure S5A). The AMP structure was identical to the one published by Silva et al. (2008) with a root-mean-square deviation (RMSD) of 0.34 Å. When we superimposed the AMP-bound structure onto our ADE-PRPP-Mg^{2+}-hAPRT structure (RMSD of 0.66 Å),

Table 1. Kinetic Parameters of the Forward and Reverse Reactions for hAPRT^{wt} and hAPRT^{Y105F}

Protein	Substrate	Apparent K_M[a] (μM)	k_{cat} (s^{-1})	k_{cat}/K_M ($M^{-1}.s^{-1}$)
hAPRT^{wt}[b]	PRPP	16.8 ± 1.8	3.85 ± 0.35	2.3 10^5
	ADE	6.1 ± 1.3		6.3 10^5
	AMP	ND	> (8 ± 0.5) 10^{-4}[c]	ND
hAPRT^{Y105F}[b]	PRPP	0.85 ± 0.20	0.013 ± 0.003	1.5 10^4
	ADE	2.9 ± 0.5		4.5 10^3
	AMP	ND	> (8 ± 0.5) 10^{-4}[c]	ND
hAPRT^{wt}[d]	ADE	6.3 ± 2.0	0.26 ± 0.03	4.1 10^4
hAPRT^{Y105F}[d]	ADE	4.7 ± 1.2	0.012 ± 0.001	2.6 10^3
Protein	Inhibitor	Apparent K_i (μM)	k_{cat} (s^{-1})	k_{cat}/K_M ($M^{-1}.s^{-1}$)
hAPRT^{wt}[b]	AMP (vs PRPP)	23 ± 6		
hAPRT^{Y105F}[b]	AMP (vs PRPP)	2.1 ± 0.6		
Protein	Inhibitor	Apparent K_{eq} (μM)	k_{cat} (s^{-1})	k_{cat}/K_M ($M^{-1}.s^{-1}$)
hAPRT^{wt}[b]		16 ± 4		
hAPRT^{Y105F}[b]		18 ± 10		

The values were calculated from the data of three independent experiments measured at 23°C, unless otherwise stated. ND, not determined. See also Figure S4.

[a]K_M, apparent Michaelis-Menten constant for adenine and PRPP using our *in vitro* spectroscopic assay.

[b]Data obtained in 100 mM Tris (pH 7.5) and 10 mM $MgCl_2$.

[c]These numbers are minimal values for the reactions due to a limited catalytic activity of the coupled reaction with human quinolinate phosphoribosyltransferase. These data were obtained at 37°C.

[d]Data obtained in crystallization solution: 85 mM Tris (pH 8.5), 5 mM $MgCl_2$, 170 mM NaOAc, 17% PEG4000 and 15% glycerol.

we found that both purine moieties were positioned in a similar way with only a small rotation on the base of about 12°. However, we observed a large change in the ribose orientation in which the C1′ atom moved by 1.8 Å from the PRPP to the AMP configuration (Figure 3C). The ribose moiety went from a 2′-endo configuration in the ADE-PRPP-Mg^{2+} complex to a 3′-exo configuration in the AMP-hAPRT structure. This also resulted in a 2′OH movement of 1.6 Å. Similar to other AMP structures (Phillips et al., 1999; Silva et al., 2008), the flexible loop in our AMP-hAPRT complex was in the open conformation with Glu104 and Tyr105 away from the active site (Figures 3D and S5B).

Tyr105 Prevents Strong Inhibition of hAPRT by AMP and Favors the Forward Reaction

Out of the 12 amino acids of the flexible loop, Glu104 and Tyr105, are strictly conserved in all species from bacteria to mammals (Figure S1B). The role of Glu104 has already been established in the *Saccharomyces cerevisiae* APRT. Glu104 is essential for catalysis since a 10^6-fold decrease in reactivity was observed with a Glu104Leu variant (Shi et al., 2001). In the *Giardia lamblia* APRT structure, as in our ADE-PRPP-Mg^{2+}-APRT (Figures 3A and S3), the glutamate hydrogen interacts with the adenine N7 nitrogen atom, and it is suspected of playing a key role in the N7 hydrogen abstraction that follows the N9-C1′ bond formation in the forward reaction (Shi et al., 2002).

The role of the Tyr105 has, however, never been investigated. In our ADE-PRPP-Mg^{2+}-APRT structure, Tyr105 is in contact with both ADE and PRPP substrates in the closed conformation of the flexible loop (Figures 3A, 3B, and S3E). It might therefore play a role in the enzyme catalytic processes.

To determine the role of this conserved residue, we produced and purified a Tyr105Phe variant, measured its kinetic properties, and compared them to the wild-type enzyme (Table 1 and Figure S4). First, we checked that the wild-type hAPRT had similar kinetic parameters compared with those previously reported for various enzymes (Bashor et al., 2002; Shi et al., 2001). Secondly, we found that, in the Tyr105Phe variant, the apparent K_M for PRPP and ADE were decreased, respectively, by 20- and 2-fold, while the k_{cat}/K_M were decreased by 15- and 140-fold, respectively. In addition, the kinetic equilibrium constant K_{eq} remained similar and around 20 for both enzymes. We then investigated the reverse reaction using a coupled reaction assay with human quinolinate phosphoribosyltransferase (hQPRT) that we purified (the plasmid was a gift from Dr. Huanting Liu and Prof. James Naismith from the University of St Andrews, Scotland). Due to a limited activity of hQPRT in our setup (k_{cat} = 0.007 ± 0.002 s^{-1}), we were unable to determine an apparent K_M value for AMP in the reverse reaction of wild-type and variant hAPRT. However, we found that both the wild-type and the hAPRT^{Y105F} variant displayed similar and minimal values for k_{cat} of 8 × 10^{-4} s^{-1} (Table 1), which were lower than those reported for *Leishmania donovani* (1.25 s^{-1}) or *Giardia lamblia* (0.01 s^{-1}) (Bashor et al., 2002; Sarver and Wang, 2002). Finally, we tested the inhibitory action of AMP on the forward reaction. We found that the Ki for AMP decreased 11-fold in the variant as compared with the wild-type enzyme (Table 1, Figures S4C and S4D). Therefore, the Tyr105Phe mutation increases the inhibitory effect of AMP while decreasing the catalytic efficiency of the enzyme in the forward reaction.

The APRT Tyr105 Drives Purine Biosynthesis *In Vivo*

We further probed the role of the Tyr105 in hAPRT by measuring cell growth of *Saccharomyces cerevisiae* in line with purine metabolism. Wild-type and mutant hAPRTs were expressed in APRT-free *Saccharomyces cerevisiae*, which is defective for *de novo* purine synthesis (strain DS1-2b, a gift from R. Woods). We found

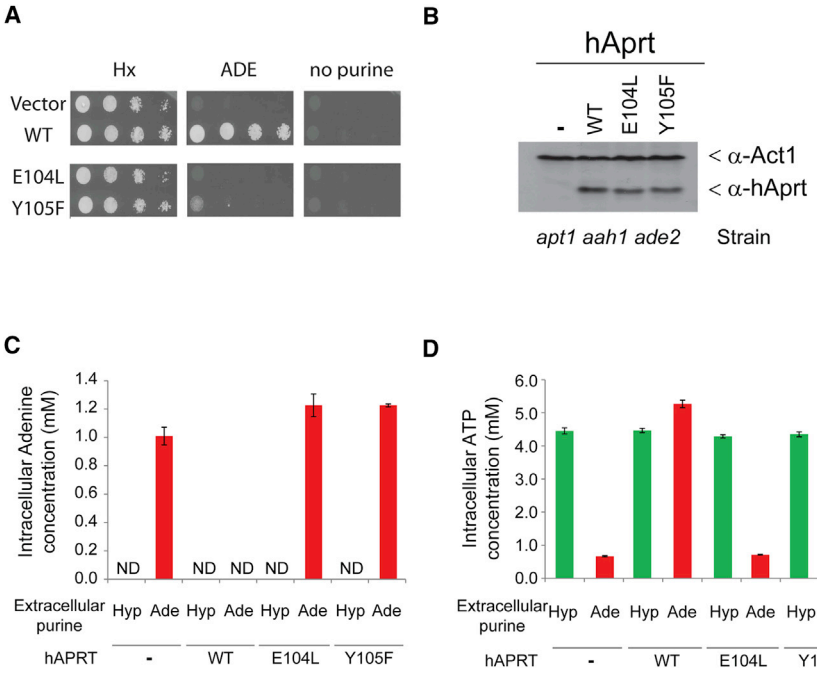

Figure 4. A Single Oxygen Atom, in the Tyr105 Side Chain, Influences Catalysis and Cell Growth

(A) Drop test viability assays in *Saccharomyces cerevisiae ade2 apt1 aah1* cells that express the indicated hAPRT variants, grown on various purine-containing media.

(B–D) (B) Protein expression was estimated from a western blot. α-Act1 corresponds to Actin antibody. Intracellular concentrations of ADE (C) and ATP (D) in the yeast strains. Cells were transformed with plasmids coding for wild-type hAPRT, variants, or by the cognate empty vector (–). Cells were grown on either adenine or hypoxanthine. ND means not detected. The reported values are best-fit means with SD representative of three measurements.

See also Figure S4.

that *Saccharomyces cerevisiae* expressing the Tyr105Phe variant of hAPRT displayed a reduced growth rate in absence of exogenous adenine, similar to the Glu104Leu variant, compared with the wild-type (Figure 4A). Despite a decrease in the kinetic efficiency of the Tyr105Phe variant, the magnitude of the low-growth phenotype observed in yeast was not anticipated. These results were not due to low protein level of the variant since its expression level was similar to the wild-type enzyme (Figure 4B). To further investigate this growth phenotype in connection with the protein activity, we measured the intracellular concentrations of ADE and ATP in the cognate strain (Figures 4C and 4D). In contrast to yeasts expressing the wild-type enzyme, we found that yeasts that expressed the Tyr105Phe variant did not process ADE. ADE concentration within the cell went up to 1 mM, as was the case in the absence of any hAPRT expression. Consequently, we observed an extremely low intracellular concentration of ATP in yeast expressing both variants (Glu104Leu or Tyr105Phe). This ATP depletion is sufficient to prevent cell growth. Similarly, the concentrations of AMP were found to be 95 ± 7, 199 ± 17, 84 ± 20, and 87 ± 17 μM, respectively, for cells transformed with an empty vector or with plasmids allowing the expression of either $hAPRT^{WT}$, $hAPRT^{E104L}$, or $hAPRT^{Y105F}$. As a whole, these data indicate that Tyr105 of the hAPRT catalytic flexible loop is critical to drive the enzyme in the forward reaction and to fuel the production of ATP necessary for cell growth.

In Crystallo Activity Shows that the Hydroxyl Group of Tyr105 Is Essential to Select the Bioactive Conformation of the Dynamic Flexible Loop and to Form the Products

To gain structural insights into our cellular and kinetic results from the Tyr105Phe variant and to investigate which determinants are important for the enzyme turnover *in crystallo*, $hAPRT^{Y105F}$ was co-crystallized with ADE and PRPP in the presence of magnesium ions (Table S2). Fourteen hours post crystallization, the crystals were harvested and frozen in liquid nitrogen. The structure (called $hAPRT^{Y105F–14hours}$) showed that Phe105 did not cap the ADE moiety as it does in ADE-PRPP-Mg^{2+}-hAPRT wild-type structures. Instead, the flexible loop was in an open conformation and superimposable on the loop conformation found in the PRPP-Mg^{2+}- and AMP-hAPRT structures (Figure 5A). In addition, although PRPP was fully defined with a position identical to that in the PRPP-Mg^{2+}-hAPRT structure, ADE was not visible in the electron density map (Figures S6A and S6B).

Fortuitously, we observed that, unlike the wild-type enzyme crystals, the crystals of the $hAPRT^{Y105F}$ variant cracked within 2 weeks (Figures S6C and S6D). Despite their appearance, these crystals still diffracted X-rays to 1.55 Å resolution (Table S2), 14 days after crystallization at 20°C (this structure is called $hAPRT^{Y105F–14days}$). The molecules in the asymmetric unit showed clear differences. The first $hAPRT^{Y105F–14days}$ subunit was bound to AMP, PPi, and Mg^{2+} (Figure 5B), with the two latter molecules having 50% occupancy. In the second subunit, PRPP and Mg^{2+} were still largely present along with a density corresponding to AMP having about 30% occupancy (Figure 5C), which indicated a lower accumulation of the product in this subunit. To further validate our findings, we collected data on the same type of crystals, 30 days post crystallization at 20°C (this structure is called $hAPRT^{Y105F–30days}$). In this case, in the first subunit, the AMP and PPi molecules were superimposable to the ones after 14 days with identical occupancy; however, no magnesium could be identified (Figure S7). In the second subunit, AMP, PPi, and Mg^{2+} were all present and their occupancy levels reached 100%, 60%, and 60%, respectively (Figure 5D). This structure is superimposable to the first $hAPRT^{Y105F–14days}$ subunit with an RMSD of 0.4 Å.

These results demonstrate that an enzymatic reaction has occurred *in crystallo* without any inducer. This *in crystallo* enzymatic activity operates even though no density for the adenine substrate was initially observed in the $hAPRT^{Y105F–14hours}$ structure. These structures further show that a single oxygen atom on

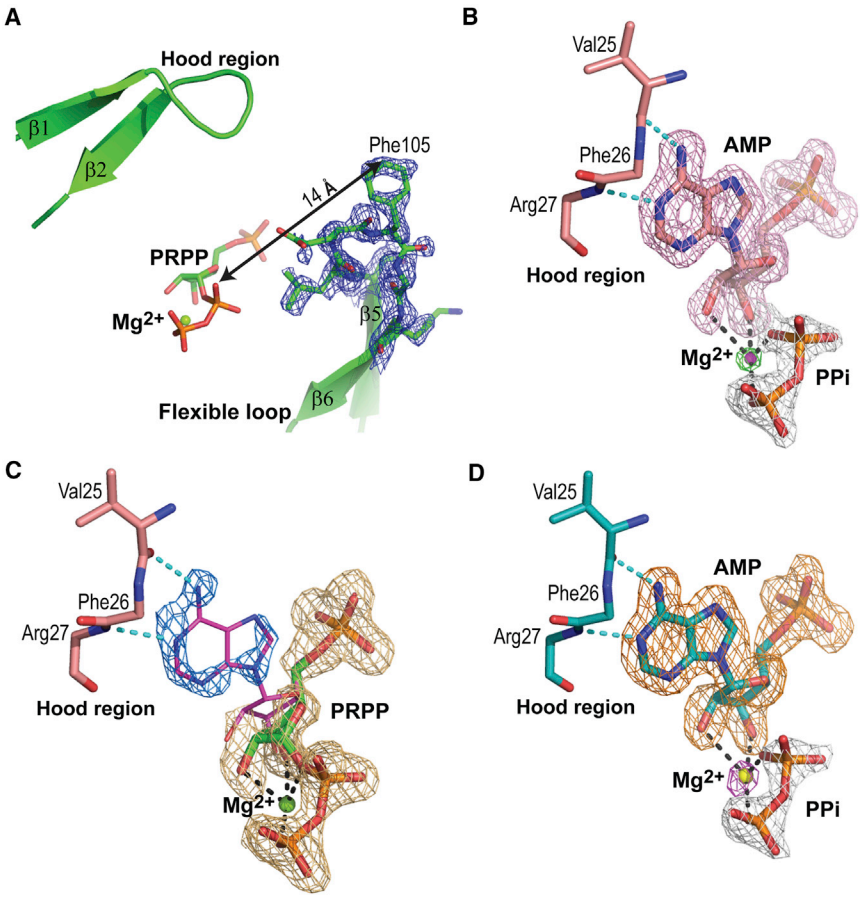

Figure 5. The Evolutionary Conserved Tyr105 Is Essential for Loop Dynamics, Active Site Formation and *In Crystallo* Catalysis

(A–C) (A) $F_o - F_c$ omit electron density map for residues 102 to 107 contoured at 3σ of the ADE-PRPP-Mg^{2+}-$hAPRT^{Y105F-14h}$ structure. $F_o - F_c$ omit electron density maps contoured at 3σ of the ADE-PRPP- Mg^{2+}-$hAPRT^{Y105F-14days}$ complex with AMP, Mg^{2+}, and PPi in one molecule (B) and AMP, Mg^{2+}, and PRPP in the second molecule (C) of the same homodimer.

(D) $F_o - F_c$ omit electron density maps for AMP and PPi contoured at 3σ for the second molecule of the ADE-PRPP-Mg^{2+}-$hAPRT^{Y105F-30days}$ complex. The electron density maps for the magnesium ion (B and D) are contoured at 6σ. Water molecules coordinating the magnesium ions are not shown for clarity.

See also Figures S6, S7, and Table S2.

the Tyr105 side chain is responsible for selecting the conformation of the 12-amino-acid-long dynamic loop and thereby generating the active site of hAPRT. Accordingly, we showed that the reaction occurs in a solvent with the same composition as the crystallization solution. However, the k_{cat}/K_M value decreased by 16-fold as compared with that of the wild-type $hAPRT^{wt}$ (Table 1, Figures S4A and S4B).

DISCUSSION

Key Features of hAPRT for Substrates Binding in the Forward and Reverse Reactions

First, our DSF analysis indicates that the binding of PRPP markedly stabilizes the enzyme in solution as compared with the unbound form. This could be due to the numerous hydrogen bonds formed by the PRPP-Mg^{2+} chelate with the enzyme (Figure 2B). Interestingly, in all our crystal structures, the conserved Asp65-Ser66 peptide bonds are in the *cis* conformation. In the substrate-free yeast APRT structure, a *cis* bond has been observed (Shi et al., 2001), while a *trans* peptide bond was found in substrate-free APRT from *Giardia lamblia* (Shi et al., 2002) or modeled in HGXPRT from *Plasmodium falciparum* (Roy et al., 2015). We hypothesize that both conformations exist in solution for the unliganded hAPRT. PRPP then selects the *cis* state of hAPRT while binding to the active site. This phenomenon likely contributes to the high protein stability observed after PRPP binding.

Second, in spite of being a less efficient variant enzyme in the forward reaction, $hAPRT^{Y105F}$ binds PRPP 20 times tighter (Table 1). In parallel, the inhibitory effect of AMP increases 11-fold, showing that the variant also binds AMP with much higher affinity than the wild-type enzyme. These results suggest that one of the roles of Tyr105 is to prevent the strong inhibition of the forward reaction by AMP. In addition, since the k_{cat} of the reverse reaction is similar in both the wild-type and variant enzymes, the $hAPRT^{Y105F}$ catalytic efficiency of the reverse reaction will be greater than in the wild-type. Finally, in the forward reaction, Tyr105 may also help the departure of AMP after catalysis.

Thirdly, our ADE-PRPP-Mg^{2+}-$hAPRT^{wt}$ structure revealed critical roles for both the hood region and the catalytic flexible loop (Figure 3B). PRPP was unable to affect the conformation of these features by itself. ADE, however, when bound to the active site with PRPP, selects the loop and the hood to close into an active conformation and to isolate ADE from the solvent. The only atoms accessible to water molecules within a 4 Å distance were the ones from the amino group at the C6 position of ADE, which are away from the chemical reaction. By inspecting the contacts made by the residues in the loop (Ala99 to Leu110), we identified Glu104 and Tyr105 as being the major contributors to this movement through the creation of new hydrogen bonds and van der Waals contacts. To date, we and others have shown that they are the only amino acid strictly conserved in the flexible loop from prokaryotes to mammals (Figure S1B) (Phillips et al., 1999; Shi et al., 2001). Together with their movement toward the adenine and PRPP substrates, the aforementioned elements are in favor of a critical role in the enzymatic reaction for these residues, confirmed by a large decrease in the k_{cat} value in our Tyr105Phe variant (Table 1). The hood and loop movements, which transform the active site into a productive conformation, constitute the second strategy used by the enzyme to establish selectivity after the *cis-trans* selection.

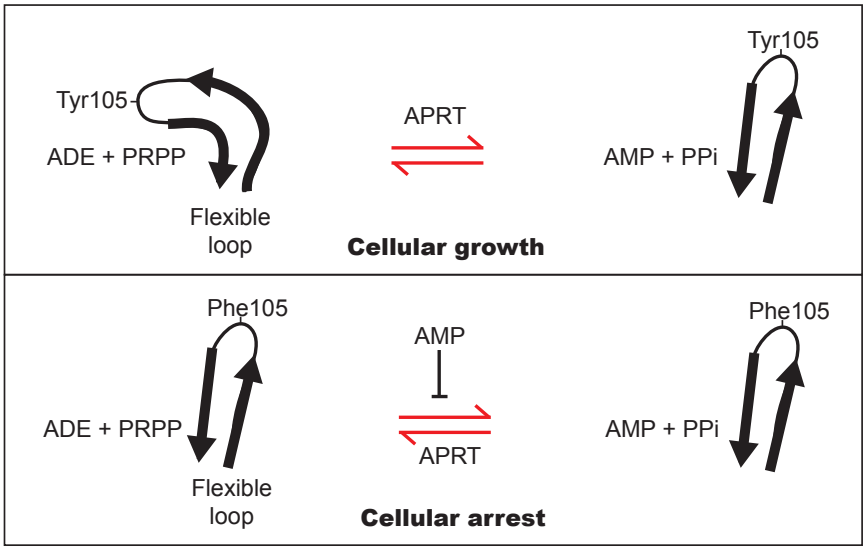

Figure 6. Model Showing a Global Evolutionary Role of Tyr105 in APRTs

Tyr105 favors cellular growth as a consequence of a flexible loop closing and limiting AMP inhibitory effect in the forward reaction. See also Figure S4.

Tyr105 Controls the Dynamics of the Catalytic Flexible Loop

Our kinetic analysis showed that the catalytic efficiency in the forward reaction is decreased by 15- and 140-fold for the PRPP and ADE substrates, respectively (Table 1). This is slightly higher than the observation of Shi et al. (2001), who showed that the equivalent yeast APRT Tyr107Phe variant enzyme exhibited a k_{cat}/K_M ratio that was decreased by 8- and 15-fold, respectively, for PRPP and ADE, compared with the wild-type enzyme. Several other studies suggested that Tyr105 could play a critical role in the formation of AMP by isolating the active site from water or by modifying the dynamics of the flexible loop (Jardim and Ullman, 1997; Schumacher et al., 1996; Shi et al., 2001). With the aim of exploring the role of Tyr105 in hAPRT activity at the structural level, we first noticed that, in the wild-type ADE-PRPP-hAPRT crystals, the catalytic reaction did not occur, even 14 days post crystallization (Figures 3A, 3B, and S3). This was surprising, firstly, because the distance between the N9 from ADE and the C1′ from PRPP was only 3.2 Å, and, secondly, all the components needed for the reaction to occur were present within the crystal. In addition, we found that the enzyme can catalyze the reaction in a solvent with the same composition as in the crystallization mixture (Figure S4A and Table 1). By investigating the macromolecular contacts, we observed that, out of the four flexible loops present in the asymmetric unit, three were not in contact with any symmetric molecules and were potentially able to move in the solvent. If modeled in the open state, the remaining loop would only contact Asp3 in the N terminus of a symmetric molecule. The loop should therefore be able to freely move away in a solvent channel. Therefore, crystal packing is neither involved in preventing the wild-type flexible loop from adopting an open conformation nor in preventing catalysis. The ADE-PRPP-Mg^{2+}-$hAPRT^{wt}$ enzyme is locked in a yet-unexplained substrate-bound state within the crystal and cannot evolve to form the expected AMP and PPi products. The key elements to understand the way the reaction proceeds further has not yet been described in the PRTases literature. An answer comes from our analysis of the high-resolution ADE-PRPP-Mg^{2+}-$hAPRT^{Y105F}$ structures obtained at different times after crystallization. At 14 hr post crystallization, PRPP was clearly seen in the electron density map at 1.55 Å resolution, whereas the second substrate, ADE, was invisible despite a concentration in the crystallization drop identical to the one used for the crystallization of the wild-type enzyme (Figures S6A and S6B). In the $hAPRT^{Y105F–14hours}$ structure, the flexible loop was in an open conformation, identical to that observed in our PRPP- Mg^{2+}- and AMP-hAPRT wild-type structures. By analyzing similar crystals 14 days or a month later, we clearly identified both AMP and PPi, in the two subunits of the asymmetric unit (Figures 5B–5D and S7). The forward reaction proceeded fully *in crystallo* to generate the products for this variant enzyme, and the substrates ADE and PRPP were consumed. Surprisingly, the catalytic efficiency of the wild-type enzyme is 16 times higher in the crystallization conditions than the variant enzyme in the forward reaction (Table 1), yet the reaction was not favored in the wild-type protein crystal.

Within the crystal of the variant, the loop may transiently adopt a closed conformation, thereby allowing ADE to react with PRPP. The loop would then move to the open conformation to allow AMP and PPi to form after the Glu104 proton transfer. This process is possible as loop opening is favored when Tyr105 is replaced by a phenylalanine. This reaction populates the active site with the products in either a single turnover process or upon the accumulation of products during several catalytic cycles. We observed that the PRPP-Mg^{2+} and ADE-PRPP-Mg^{2+}-bound complexes have identical melting temperatures (Table S1). The enzyme with its loop in an open conformation (PRPP-Mg^{2+}-bound) is, therefore, as thermostable as one with its loop in the closed conformation (ADE-PRPP-Mg^{2+}-bound). These results are consistent with the 12,000 s^{-1} rate of loop closure, determined by NMR, during the dynamic motion of the flexible loop in wild-type *Salmonella typhimurium* Orotate PRT (OPRT) bound to PRPP (Wang et al., 1999). Hence, in a solution, the loop swings easily from one conformation to the other.

We conclude that the enzymatic reaction requires dynamic loop behavior and that it has to open to generate AMP and PPi from adenine and PRPP. The presence of Tyr105 shifts the loop to a closed conformation in the presence of an ADE-shaped substrate, favoring the forward reaction. Then, the protonation of Glu104 and the loop dynamics promote the formation and release of products. The interaction of the Tyr105 hydroxyl group with the 1′-pyrophosphate moiety and Arg67 is the key to stabilize the closed conformation and generate the products of the forward reaction (Figure 6). This interaction is absent in the Phe105 variant enzyme, which will preferentially select the

open conformation. The latter will allow the enzymatic reaction to proceed *in crystallo*.

It is well established that enzymatic reactions and protein conformational changes can occur in the crystalline state. Some of the first examples were reported in the 1960s while studying globins (Chance et al., 1966; Perutz et al., 1964). More recently, *in crystallo* enzymatic reactions have been reported in a few other systems. In these instances, the reaction was induced by X-rays (Berglund et al., 2002), through changes in the oxidative environment (Yi et al., 2010), or by the addition of a ligand (Hill et al., 2013; Jackson et al., 2008; Jensen et al., 2010). Yet, our study reports an unusual *in crystallo* enzymatic reaction that is firstly, not observed in the wild-type protein but induced by a single mutation, and secondly, proceeds in the crystal without the addition of other elements into the system.

In the Forward Reaction, Tyr105 Controls the Inhibitory Role of AMP in Cells

The removal of the hydroxyl group from Tyr105, makes the enzyme less efficient in the forward reaction, while it is the opposite in the reverse reaction (Table 1 and Figure S4). These results demonstrate that the open conformation of the loop favors the reverse reaction by increasing its catalytic efficiency. It fully correlates with our nucleotide complex structures in which the AMP substrate interacts with hAPRT having the flexible loop in its open conformation. It also correlates with our *in vivo* yeast viability assay. Indeed, in the Tyr105Phe variant yeast, we found that the intracellular concentration of adenine was 1 mM. The substrate is therefore bioavailable for $hAPRT^{Y105F}$, which has a K_M of 2.9 μM. In addition, the intracellular concentration of AMP is about 85 μM. Under similar conditions (Figure S4D), $hAPRT^{Y105F}$ has a K_i for AMP versus PRPP 40 times lower (2.1 μM) than the concentration of AMP within cells (Table 1). This makes AMP a saturating substrate for $hAPRT^{Y105F}$, and to a lesser extent $hAPRT^{wt}$. Since the binding site is specific to AMP and not to other nucleoside monophosphates, such as IMP or GMP (with Ki of around 200 μM; Murray, 1967), AMP must act as an inhibitor of the forward reaction for the $hAPRT^{Y105F}$ variant in which the flexible loop preferentially stays in the open conformation. Hence, in the presence of AMP, the forward reaction cannot occur resulting in an accumulation of ADE and a large depletion of ATP along with a concomitant decrease in cell growth (Figures 4A, 4C, and 4D). These results illustrate the evolutionary selection pressure to strictly conserve Tyr105 in APRT in all organisms, from prokaryotes to eukaryotes (Figure S1B). Other amino acids in the flexible loop may also contribute to control its dynamic function and the kinetic parameters of the forward and reverse reaction. Further structural and biochemical studies would be needed to identify them. In summary, the forward reaction in APRT is under the control of ADE, PRPP, and AMP concentrations, the latter acting as a feedback mechanism under the control of both the tyrosine 105 and the flexible loop dynamics.

Conclusions

Our findings enabled us to identify a key residue in hAPRT that effects the catalytic efficiencies of both the forward and reverse reactions in order to sustain cell survival when adenine is the sole purine source. This residue has been strictly conserved through evolution to control catalysis and the dynamics of the flexible loop. We also show an *in crystallo* catalytic activity induced by a change in protein dynamics and specificity. Finally, since N6 in adenine is the only atom exposed to water molecule within a 4 Å radius in the ADE-PRPP-Mg^{2+}-$hAPRT^{wt}$ structure, this chemical group can be modified to give novel adenine analogs with specific functions. These analog modifications could be easily performed using our ADE-PRPP-Mg^{2+}-$hAPRT^{wt}$ structure as template. Such a compound like cytokinin nucleobases are also substrates of plant APRTs and they play an important role in plant development (Zhang et al., 2013). In addition, a similar analog affects the Parkinson-disease-related kinase (PINK1) pathway. This analog is the precursor of KMP through hAPRT (Hertz et al., 2013). Together with recently solved PINK1 structures (Kumar et al., 2017; Schubert et al., 2017), our data provide a scaffold to explore small molecule modulators of the PINK1 pathway.

SIGNIFICANCE

The recycling of purines, through the salvage pathway, is an important process for cell homeostasis. It participates in nucleic acid synthesis, energy-dependent reactions, and cellular signaling. The structures of human adenine phosphorybosyltransferase (hAPRT) reveal its substrate's specificity in both directions of the reaction along with a dynamic motion of its catalytic loop. Our kinetic and structural analyses of a structure-based variant provide a rationale for the central role of a conserved tyrosine in kinetic parameters' control of the forward and reverse enzyme activities. These findings give new opportunities to modulate the activities of other members of the PRT family. These data also provide the framework to design other adenine derivatives modified at the N6 position. These compounds will be processed by hAPRT and used to regulate other pathways within cells. This strategy has already been observed in the Parkinson-disease-related kinase (PINK1) or plant cytokinins pathways and could therefore be developed with potential applications in crop development or cure for neuronal diseases in humans.

STAR★METHODS

Detailed methods are provided in the online version of this paper and include the following:

- KEY RESOURCES TABLE
- CONTACT FOR REAGENT AND RESOURCES SHARING
- EXPERIMENTAL MODEL AND SUBJECT DETAILS
- METHOD DETAILS
  - Protein Purification and Crystallization
  - Data Collection, Processing and Structure Refinement
  - Differential Scanning Fluorimetry Assays
  - *In Vitro* hAPRT Kinetic Analysis
  - *APRT* Mutagenesis
  - Yeast Medium, Growth Tests and Metabolite Determinations
- QUANTIFICATION AND STATISTICAL ANALYSIS
- DATA AND SOFTWARE AVAILABILITY

SUPPLEMENTAL INFORMATION

Supplemental Information includes seven figures, one scheme, and two tables and can be found with this article online at https://doi.org/10.1016/j.chembiol.2018.02.011.

ACKNOWLEDGMENTS

We are grateful to the staffs at the X-ray crystallography beamlines of SOLEIL and ESRF. In particular, we thank the staff of ID30a at ESRF (Massif 1) who allowed us to test this fully automatic beamline while still in development. We thank Drs. Lawrence Aggerbeck, Olivia Reinaud, Mélanie Ethève-Quelquejeu, C.S. Raman, Kwame Amaning, and Benoit Schneider for their very useful reading and discussion of the manuscript. This work was supported in part by the French National Research Agency (2010-CESA-015 to J.H. and P.N.), the ARC Foundation (M.O.), an Inserm-University Chair (P.N.), Paris City Hall and Ile de France Region grants (P.N.) and two research contracts from Sanofi (116048 to I.C.P., B.P., and B.D.F., EU-TL-2013-003 to P.N.). P.N. also thanks Athéna Amayed for her support.

AUTHOR CONTRIBUTIONS

M.C.B. and F.C. performed the early kinetic analyses, which were finalized by P.N. J.M.R. and R.M. measured and analyzed the DLS data. J.F.G. did early modeling. I.C.P., R.B., and A.O.B. initiated the project and discussed the results. C.S.M., B.P., and B.D.F. performed the mutational analyses and yeast assays, and discussed the results. F.A. initiated the project, discussed the results, and wrote the paper. A.R.S., R.L., and G.P. discussed the results and wrote the paper. J.H., M.O., and P.N. crystallized the proteins, collected and analyzed the data, discussed the results, and wrote the paper.

DECLARATION OF INTERESTS

The authors declare no competing financial interest.

Received: June 1, 2017
Revised: January 5, 2018
Accepted: February 22, 2018
Published: March 22, 2018

REFERENCES

Bashor, C., Denu, J.M., Brennan, R.G., and Ullman, B. (2002). Kinetic mechanism of adenine phosphoribosyltransferase from *Leishmania donovani*. Biochemistry *41*, 4020–4031.

Berens, R.L., Krug, E.C., and Marr, J. (1995). Purine and pyrimidine metabolism. In Biochemistry and Molecular Biology of Parasites, J. Marr and M. Müller, eds. (Elsevier), pp. 89–117.

Berglund, G.I., Carlsson, G.H., Smith, A.T., Szoke, H., Henriksen, A., and Hajdu, J. (2002). The catalytic pathway of horseradish peroxidase at high resolution. Nature *417*, 463–468.

Bollee, G., Dollinger, C., Boutaud, L., Guillemot, D., Bensman, A., Harambat, J., Deteix, P., Daudon, M., Knebelmann, B., and Ceballos-Picot, I. (2010). Phenotype and genotype characterization of adenine phosphoribosyltransferase deficiency. J. Am. Soc. Nephrol. *21*, 679–688.

Bollee, G., Harambat, J., Bensman, A., Knebelmann, B., Daudon, M., and Ceballos-Picot, I. (2012). Adenine phosphoribosyltransferase deficiency. Clin. J. Am. Soc. Nephrol. *7*, 1521–1527.

Ceballos-Picot, I., and Jinnah, H.A. (2016). Disorders of purine metabolism affecting adults. In Inherited Metabolic Disease in Adults - A Clinical Guide, C.E.M. Hollak and R. Lachmann, eds. (Oxford University Press), pp. 251–263.

Ceballos-Picot, I., Daudon, M., Harambat, J., Bensman, A., Knebelmann, B., and Bollée, G. (2014). 2,8-Dihydroxyadenine urolithiasis: a not so rare inborn error of purine metabolism. Nucleosides Nucleotides Nucleic Acids *33*, 241–252.

Ceballos-Picot, I., Le Dantec, A., Brassier, A., Jais, J.P., Ledroit, M., Cahu, J., Ea, H.K., Daignan-Fornier, B., and Pinson, B. (2015). New biomarkers for early diagnosis of Lesch-Nyhan disease revealed by metabolic analysis on a large cohort of patients. Orphanet J. Rare Dis. *10*, 7.

Ceschin, J., Saint-Marc, C., Laporte, J., Labriet, A., Philippe, C., Moenner, M., Daignan-Fornier, B., and Pinson, B. (2014). Identification of yeast and human 5-aminoimidazole-4-carboxamide-1-beta-d-ribofuranoside (AICAr) transporters. J. Biol. Chem. *289*, 16844–16854.

Chance, B., Ravilly, A., and Rumen, N. (1966). Reaction kinetics of a crystalline hemoprotein: an effect of crystal structure on reactivity of ferrimyoglobin. J. Mol. Biol. *17*, 525–534.

Colowick, S.P., Kaplan, N.O., and Ciotti, M.M. (1951). The reaction of pyridine nucleotide with cyanide and its analytical use. J. Biol. Chem. *191*, 447–459.

Curto, R., Voit, E.O., Sorribas, A., and Cascante, M. (1997). Validation and steady-state analysis of a power-law model of purine metabolism in man. Biochem. J. *324* (Pt 3), 761–775.

Deller, M.C., and Rupp, B. (2015). Models of protein–ligand crystal structures: trust, but verify. J. Comput. Aided Mol. Des. *29*, 817–836.

Eads, J.C., Scapin, G., Xu, Y., Grubmeyer, C., and Sacchettini, J.C. (1994). The crystal structure of human hypoxanthine-guanine phosphoribosyltransferase with bound GMP. Cell *78*, 325–334.

Emsley, P., Lohkamp, B., Scott, W.G., and Cowtan, K. (2010). Features and development of Coot. Acta Crystallogr. D Biol. Crystallogr. *66*, 486–501.

Escusa, S., Camblong, J., Galan, J.M., Pinson, B., and Daignan-Fornier, B. (2006). Proteasome- and SCF-dependent degradation of yeast adenine deaminase upon transition from proliferation to quiescence requires a new F-box protein named Saf1p. Mol. Microbiol. *60*, 1014–1025.

Evans, P.R., and Murshudov, G.N. (2013). How good are my data and what is the resolution? Acta Crystallogr. D Biol. Crystallogr. *69*, 1204–1214.

Gari, E., Piedrafita, L., Aldea, M., and Herrero, E. (1997). A set of vectors with a tetracycline-regulatable promoter system for modulated gene expression in *Saccharomyces cerevisiae*. Yeast *13*, 837–848.

Gutierrez, J.A., Crowder, T., Rinaldo-Matthis, A., Ho, M.C., Almo, S.C., and Schramm, V.L. (2009). Transition state analogs of 5′-methylthioadenosine nucleosidase disrupt quorum sensing. Nat. Chem. Biol. *5*, 251–257.

Heinonen, J.K. (2001). Biological Role of Inorganic Pyrophosphate (Springer).

Hertz, N.T., Berthet, A., Sos, M.L., Thorn, K.S., Burlingame, A.L., Nakamura, K., and Shokat, K.M. (2013). A neo-substrate that amplifies catalytic activity of Parkinson's-disease-related kinase PINK1. Cell *154*, 737–747.

Hill, C.H., Graham, S.C., Read, R.J., and Deane, J.E. (2013). Structural snapshots illustrate the catalytic cycle of beta-galactocerebrosidase, the defective enzyme in Krabbe disease. Proc. Natl. Acad. Sci. USA *110*, 20479–20484.

Jackson, C.J., Foo, J.L., Kim, H.K., Carr, P.D., Liu, J.W., Salem, G., and Ollis, D.L. (2008). In crystallo capture of a Michaelis complex and product-binding modes of a bacterial phosphotriesterase. J. Mol. Biol. *375*, 1189–1196.

Jardim, A., and Ullman, B. (1997). The conserved serine-tyrosine dipeptide in *Leishmania donovani* hypoxanthine-guanine phosphoribosyltransferase is essential for catalytic activity. J. Biol. Chem. *272*, 8967–8973.

Jensen, L.M., Sanishvili, R., Davidson, V.L., and Wilmot, C.M. (2010). In crystallo posttranslational modification within a MauG/pre-methylamine dehydrogenase complex. Science *327*, 1392–1394.

Kabsch, W. (2010). Xds. Acta Crystallogr. D Biol. Crystallogr. *66*, 125–132.

Kabsch, W., and Sander, C. (1983). Dictionary of protein secondary structure: pattern recognition of hydrogen-bonded and geometrical features. Biopolymers *22*, 2577–2637.

Khan, J.A., Tao, X., and Tong, L. (2006). Molecular basis for the inhibition of human NMPRTase, a novel target for anticancer agents. Nat. Struct. Mol. Biol. *13*, 582–588.

Kumar, A., Tamjar, J., Waddell, A.D., Woodroof, H.I., Raimi, O.G., Shaw, A.M., Peggie, M., Muqit, M.M., and van Aalten, D.M. (2017). Structure of PINK1 and mechanisms of Parkinson's disease-associated mutations. Elife *6*, https://doi.org/10.7554/eLife.29985.

Leslie, A.G.W., and Powell, H.R. (2007). Processing diffraction data with MOSFLM. Evol. Methods Macromol. Crystallogr. *245*, 41–51.

Liu, H., Woznica, K., Catton, G., Crawford, A., Botting, N., and Naismith, J.H. (2007). Structural and kinetic characterization of quinolinate phosphoribosyltransferase (hQPRTase) from homo sapiens. J. Mol. Biol. *373*, 755–763.

McCoy, A.J., Grosse-Kunstleve, R.W., Adams, P.D., Winn, M.D., Storoni, L.C., and Read, R.J. (2007). Phaser crystallographic software. J. Appl. Crystallogr. *40*, 658–674.

Murray, A.W. (1967). Studies on the nature of the regulation by purine nucleotides of adenine phosphoribosyltransferase and of hypoxanthine phosphoribosyltransferase from Ehrlich ascites-tumour cells. Biochem. J. *103*, 271–279.

Murshudov, G.N., Vagin, A.A., and Dodson, E.J. (1997). Refinement of macromolecular structures by the maximum-likelihood method. Acta Crystallgr. D Biol. Crystallgr. *53*, 240–255.

Niesen, F.H., Berglund, H., and Vedadi, M. (2007). The use of differential scanning fluorimetry to detect ligand interactions that promote protein stability. Nat. Protoc. *2*, 2212–2221.

Nyhan, W.L. (2005a). Disorders of purine and pyrimidine metabolism. Mol. Genet. Metab. *86*, 25–33.

Nyhan, W.L. (2005b). Inherited hyperuricemic disorders. Contrib. Nephrol. *147*, 22–34.

Perutz, M.F., Bolton, W., Diamond, R., Muirhead, H., and Watson, H.C. (1964). Structure of haemoglobin. An X-ray examination of reduced horse haemoglobin. Nature *203*, 687–690.

Phillips, C.L., Ullman, B., Brennan, R.G., and Hill, C.P. (1999). Crystal structures of adenine phosphoribosyltransferase from *Leishmania donovani*. EMBO J. *18*, 3533–3545.

Pillwein, K., Chiba, P., Knoflach, A., Czermak, B., Schuchter, K., Gersdorf, E., Ausserer, B., Murr, C., Goebl, R., Stockhammer, G., et al. (1990). Purine metabolism of human glioblastoma in vivo. Cancer Res. *50*, 1576–1579.

Roy, S., Karmakar, T., Prahlada Rao, V.S., Nagappa, L.K., Balasubramanian, S., and Balaram, H. (2015). Slow ligand-induced conformational switch increases the catalytic rate in *Plasmodium falciparum* hypoxanthine guanine xanthine phosphoribosyltransferase. Mol. Biosyst. *11*, 1410–1424.

Saint-Marc, C., Pinson, B., Coulpier, F., Jourdren, L., Lisova, O., and Daignan-Fornier, B. (2009). Phenotypic consequences of purine nucleotide imbalance in *Saccharomyces cerevisiae*. Genetics *183*, 529–538, 1SI–7SI.

Sarver, A.E., and Wang, C.C. (2002). The adenine phosphoribosyltransferase from *Giardia lamblia* has a unique reaction mechanism and unusual substrate binding properties. J. Biol. Chem. *277*, 39973–39980.

Schubert, A.F., Gladkova, C., Pardon, E., Wagstaff, J.L., Freund, S.M.V., Steyaert, J., Maslen, S.L., and Komander, D. (2017). Structure of PINK1 in complex with its substrate ubiquitin. Nature *552*, 51–56.

Schumacher, M.A., Carter, D., Roos, D.S., Ullman, B., and Brennan, R.G. (1996). Crystal structures of *Toxoplasma gondii* HGXPRTase reveal the catalytic role of a long flexible loop. Nat. Struct. Biol. *3*, 881–887.

Shi, W., Li, C.M., Tyler, P.C., Furneaux, R.H., Grubmeyer, C., Schramm, V.L., and Almo, S.C. (1999). The 2.0 A structure of human hypoxanthine-guanine phosphoribosyltransferase in complex with a transition-state analog inhibitor. Nat. Struct. Biol. *6*, 588–593.

Shi, W., Tanaka, K.S., Crother, T.R., Taylor, M.W., Almo, S.C., and Schramm, V.L. (2001). Structural analysis of adenine phosphoribosyltransferase from *Saccharomyces cerevisiae*. Biochemistry *40*, 10800–10809.

Shi, W., Sarver, A.E., Wang, C.C., Tanaka, K.S., Almo, S.C., and Schramm, V.L. (2002). Closed site complexes of adenine phosphoribosyltransferase from *Giardia lamblia* reveal a mechanism of ribosyl migration. J. Biol. Chem. *277*, 39981–39988.

Sievers, F., Wilm, A., Dineen, D., Gibson, T.J., Karplus, K., Li, W., Lopez, R., McWilliam, H., Remmert, M., Söding, J., et al. (2011). Fast, scalable generation of high-quality protein multiple sequence alignments using Clustal Omega. Mol. Syst. Biol. *7*, 539.

Silva, C.H., Silva, M., Iulek, J., and Thiemann, O.H. (2008). Structural complexes of human adenine phosphoribosyltransferase reveal novel features of the APRT catalytic mechanism. J. Biomol. Struct. Dyn. *25*, 589–597.

Silva, M., Silva, C.H., Iulek, J., and Thiemann, O.H. (2004). Three-dimensional structure of human adenine phosphoribosyltransferase and its relation to DHA-urolithiasis. Biochemistry *43*, 7663–7671.

Terkeltaub, R. (2012). Gout and Other Crystal Arthropathies (Elsevier Saunders).

Tuttle, J.V., and Krenitsky, T.A. (1980). Purine phosphoribosyltransferases from *Leishmania donovani*. J. Biol. Chem. *255*, 909–916.

de Vries, A., and Sperling, O. (1977). Implications of disorders of purine metabolism for the kidney and the urinary tract. Ciba Found. Symp. *48*, 179–206.

Wang, G.P., Cahill, S.M., Liu, X., Girvin, M.E., and Grubmeyer, C. (1999). Motional dynamics of the catalytic loop in OMP synthase. Biochemistry *38*, 284–295.

Weber, G., Jayaram, H.N., Pillwein, K., Natsumeda, Y., Reardon, M.A., and Zhen, Y.S. (1987). Salvage pathways as targets of chemotherapy. Adv. Enzyme Regul. *26*, 335–352.

Winn, M.D., Ballard, C.C., Cowtan, K.D., Dodson, E.J., Emsley, P., Evans, P.R., Keegan, R.M., Krissinel, E.B., Leslie, A.G., McCoy, A., et al. (2011). Overview of the CCP4 suite and current developments. Acta Crystallogr. D Biol. Crystallogr. *67*, 235–242.

Yi, C.Q., Jia, G.F., Hou, G.H., Dai, Q., Zhang, W., Zheng, G.Q., Jian, X., Yang, C.G., Cui, Q.A., and He, C.A. (2010). Iron-catalysed oxidation intermediates captured in a DNA repair dioxygenase. Nature *468*, 330–333.

Yuan, L., Craig, S.P., McKerrow, J.H., and Wang, C.C. (1992). Steady-state kinetics of the schistosomal hypoxanthine-guanine phosphoribosyltransferase. Biochemistry *31*, 806–810.

Zaidan, M., Palsson, R., Merieau, E., Cornec-Le Gall, E., Garstka, A., Maggiore, U., Deteix, P., Battista, M., Gagné, E.R., Ceballos-Picot, I., et al. (2014). Recurrent 2,8-dihydroxyadenine nephropathy: a rare but preventable cause of renal allograft failure. Am. J. Transpl. *14*, 2623–2632.

Zhang, X., Chen, Y., Lin, X., Hong, X., Zhu, Y., Li, W., He, W., An, F., and Guo, H. (2013). Adenine phosphoribosyl transferase 1 is a key enzyme catalyzing cytokinin conversion from nucleobases to nucleotides in Arabidopsis. Mol. Plant *6*, 1661–1672.

Zrenner, R., Stitt, M., Sonnewald, U., and Boldt, R. (2006). Pyrimidine and purine biosynthesis and degradation in plants. Annu. Rev. Plant Biol. *57*, 805–836.

STAR★METHODS

KEY RESOURCES TABLE

REAGENT or RESOURCE	SOURCE	IDENTIFIER
Antibodies		
Anti-human APRT	Abcam	Cat#Ab196558
Anti-actin	Dr. J.A. Cooper, Washington University School of Medicine, St Louis, MO, USA	N/A
Bacterial and Virus Strains		
BL21(DE3) *E. coli*	New England Biolabs	Cat#C25271
Chemicals, Peptides, and Recombinant Proteins		
$hAPRT^{wt}$	Euromedex	Cat#ATGP0483
$hAPRT^{Y105F}$	This paper	N/A
PRPP	Sigma-Aldrich	Cat#P8296
ADE	Sigma-Aldrich	Cat#01830
AMP	Sigma-Aldrich	Cat#01930
PPi	Fluka	Cat#71515
Quinolinic acid	Sigma-Aldrich	Cat#P63204
Hypoxanthine	Sigma-Aldrich	Cat#H9377
Tris-HCl	Prolabo	Cat#28808.294
NaOAc	Prolabo	Cat#27652.298
PEG4000	Fluka	Cat#81242
Glycerol	Prolabo	Cat#24388.295
Casamino acids	BD-Bioscience	Cat#223050
Tryptophan	Sigma-Aldrich	Cat#T0254
Terrific Broth media	MoBio	Cat#12105
IPTG	Euromedex	Cat#EU0008-C
Yeast nitrogen Base without aminoacids and ammonium sulfate	BD-Bioscience	Cat#233520
Q-sepharose	GE	Cat#17-0451-10
AMP-agarose	Sigma-Aldrich	Cat#A1271
Ni-NTA	GE	Cat#17-5318-02
Gel filtration column	GE	Cat#17-1069-01
PCR microplates	Roche	Cat#04729749001
Sartolon polyamide filters 0.45 μm	Sartorius stedim Biotech	Cat#25006-47-N
Carbopac PA1 column	Thermo Electron SAS	Cat#057178
Critical Commercial Assays		
SYPRO orange	Invitrogen, Carlsbad	Cat#S6651
Deposited Data		
The structure of the PRPP-Mg^{2+}-$hAPRT^{wt}$ complex	This paper	PDB_ID : 6FCH
The structure of the ADE-PRPP-Mg^{2+}-$hAPRT^{wt}$ complex	This paper	PDB_ID : 6FCI
The structure of the AMP-bound $hAPRT^{wt}$ complex	This paper	PDB_ID : 6FCL
The structure of the ADE-PRPP-Mg^{2+}-$hAPRT^{Y105F\text{-}14hours}$ complex	This paper	PDB_ID : 6FD4
The structure of the ADE-PRPP-Mg^{2+}-$hAPRT^{Y105F\text{-}14days}$ complex	This paper	PDB_ID : 6FD5
The structure of the ADE-PRPP-Mg^{2+}-$hAPRT^{Y105F\text{-}30days}$ complex	This paper	PDB_ID : 6FD6

(*Continued on next page*)

Continued		
REAGENT or RESOURCE	SOURCE	IDENTIFIER
Experimental Models: Organisms/Strains		
MATα ade2 apt1 aah1 ura3 yeast strain	Dr. R. Woods, University of Winnipeg, Winnipeg, MB, Canada	N/A
Oligonucleotides		
Forward primer for E104L mutation: 5'-CTATGGGCATCT TACTCACTTCTATATGGAAAGGCTGAACTTG-3'	This paper	N/A
Forward primer for Y105F mutation: 5'-GGGCATCTTACT CACTTGAATTTGGAAAGGCTGAACTTGAAATTC-3'	This paper	N/A
Recombinant DNA		
pET24d	Novagen	Cat#69752
pEHIShqprt	Dr. Huanting Liu and Prof. James Naismith from the University of St Andrew, Scotland	N/A
pCM189	Gari et al., 1997	N/A
hAPRT gene optimized for yeast expression	DNA2.0	N/A
Software and Algorithms		
iMOSFLM	Leslie and Powell, 2007	https://www.mrc-lmb.cam.ac.uk/harry/imosflm/ver721/introduction.html
XDS	Kabsch, 2010	http://xds.mpimf-heidelberg.mpg.de/
AIMLESS	Evans and Murshudov, 2013	http://www.ccp4.ac.uk/html/aimless.html
PHASER	McCoy et al., 2007	http://www.phenix-online.org/
REFMAC5	Murshudov et al., 1997	http://www.ccp4.ac.uk/html/refmac5.html
CCP4i	Winn et al., 2011	http://www.ccp4.ac.uk/ccp4i_main.php
COOT	Emsley et al., 2010	https://www2.mrc-lmb.cam.ac.uk/personal/pemsley/coot/
Origin 6.1	OriginLab	tps://www.originlab.com/index.aspx?go=PRODUCTS/Origin

CONTACT FOR REAGENT AND RESOURCES SHARING

Further information and requests for ressources and reagents should be directed to and will be fulfilled by the Lead Contact, Pierre Nioche (pierre.nioche@gmail.com).

EXPERIMENTAL MODEL AND SUBJECT DETAILS

Saccharomyces cerevisiae DS.1-2B/1 strain with genotype *MAT* alpha *ade2 apt1 aah1 ura3* were used in this study. Cells were grown in a SD synthetic minimal medium containing 5% ammonium sulfate, 0.17% yeast nitrogen base (Difco), 2% glucose supplemented with 0.2% casamino acids (Difco) and tryptophan (0.2 mM) and either adenine (0.3 mM) or hypoxanthine (0.3 mM).

METHOD DETAILS

Protein Purification and Crystallization

The hAPRT wild type protein was purchased from Euromedex (France) (catalog number: ATGP0483, lot: 1046601). The protein preparation was done at 4°C. The protein was diluted four times into buffer A (20 mM Tris-HCl pH 7.4, 5 mM $MgCl_2$) with a 50-fold dilution factor and concentrated each time. A final concentration to 5 $mg.ml^{-1}$ was performed as assessed by UV/visible spectroscopy using an estimated absorption coefficient ε(280 nm) = 41,200 $M^{-1}cm^{-1}$. To prepare ADE-PRPP-Mg^{2+}-$hAPRT^{wt}$ co-crystals, the protein was first mixed with a 400 mM concentrated solution of PRPP in a 20:1 volume ratio (final PRPP concentration of 20 mM). Then, a saturated solution of ADE was added in a 20:1 volume ratio. All the solutions were prepared in buffer A and the final protein concentration of the complex was 4.5 $mg.mL^{-1}$. The PRPP-Mg^{2+}-hAPRT complex was prepared by buffer exchanging hAPRT with 500 μM PRPP-containing buffer A as described above, and concentrating the complex to 11 $mg.ml^{-1}$. Using a Mosquito robot (TTP LabTec), 400 nL of each complex was mixed with 200 nL of crystallization solutions made of 85 mM Tris-HCl pH 8.5, 170 mM NaOAc and 19-21% PEG4000 mixed with 0-30 % glycerol. The plates were incubated at 20°C and crystals appeared overnight. The adenine containing

crystals were transferred to a cryo-solution made of the crystallization solutions supplemented with 25 % glycerol before being flash frozen in liquid nitrogen. PRPP-Mg^{2+}-hAPRT crystals were directly frozen in liquid nitrogen a couple of days after growth. The storage of the PRPP-Mg^{2+}-hAPRT crystals for one month at 20°C led to a complete hydrolysis of the PRPP, which left a free active site with a single phosphate ion bound. To prepare the AMP-hAPRT complex, we transferred these substrate-free crystals into crystallization solutions containing 20 mM AMP for 45 minutes. We repeated this transfer three times to insure full occupancy for AMP in the hAPRT active site. The crystals were then frozen immediately in liquid nitrogen. After cloning the gene in a pET24d plasmid, the $hAPRT^{Y105F}$ variant was induced with 0.5 mM IPTG and expressed in BL21(DE3) *E. coli* cells in Terrific Broth media (MoBio). After three days at 28°C with shaking at 100 rpm, the cells were centrifuged and frozen in liquid nitrogen. A pellet corresponding to 1.6 L culture was then mixed with 70 mL of buffer A and sonicated for 4 minutes. After centrifugation at 24,500 rpm for 45 minutes, the supernatant was diluted two-fold in buffer A and applied onto a 5mL Q sepharose (GE, 17-0510-10) column equilibrated in the same buffer. Human $APRT^{Y105F}$ eluted during an NaCl gradient at a conductivity of approximately 8 mS. The protein then was diluted 10 fold in buffer A and applied onto a 5 mL AMP-agarose resin (Sigma, A1271). The resin was washed with 30 column volumes of buffer A and the protein was eluted in 10 mL of buffer A containing 5 mM AMP. After concentrating the protein sample to 2 mL, it was applied onto a preparative gel filtration column (GE, 17-1069-01) equilibrated in buffer A which contained 150 mM NaCl. The protein eluted as a single peak with an elution volume corresponding to a dimer, as analyzed from a calibration curve. The sample was concentrated and rapidly mixed with a PRPP solution saturated with ADE in a 10:12 ratio to obtain final concentrations of 5 mg/mL of protein and 16.7 mM PRPP. The same crystallization solutions as above were then used to prepare the ADE-PRPP-$hAPRT^{Y105F}$ crystals. The human QPRT plasmid (pEHIShqprt) was a gift from Dr. Huanting Liu and Prof. James Naismith from the University of St Andrew, Scotland (Liu et al., 2007). The human QPRT (hQPRT) was induced with 0.5 mM IPTG and expressed in BL21(DE3) *E. coli* cells in Terrific Broth media. After one day at 20°C with shaking at 190 rpm, the cells were centrifuged and frozen in liquid nitrogen. A pellet corresponding to 2.4 L culture was then mixed with 90 mL of buffer B (50 mM NaH_2PO_4, pH = 7.0, 350 mM NaCl, 5% Glycerol) and sonicated for 4 minutes. After centrifugation at 24,500 rpm for 45 minutes, the supernatant was applied onto a 2 mL Ni-NTA affinity column (GE, 17-5318-02). After three washes with 50 mL of buffer B, the protein was eluted in 200 mM imidazole-containing buffer B. The sample was then concentrated to 2 mL and applied onto a preparative gel filtration column (GE, 17-1069-01) equilibrated in buffer C (50 mM KH_2PO_4, pH = 7.5, 5 mM MgCL2, 200 mM NaCl). The sample was concentrated to 2-5 mM and use rapidly in a coupled kinetic assay together with hAPRT.

Data Collection, Processing and Structure Refinement

Six diffraction data were obtained at SOLEIL (beamline PX2) and ESRF (beamlines ID14-4, ID23-2, ID29 and ID30a) (Table S2). They were integrated with iMOSFLM (Leslie and Powell, 2007) or XDS (Kabsch, 2010) and scaled with_ENREF_51 AIMLESS (Evans and Murshudov, 2013). The PRPP-Mg^{2+}-hAPRT structure was obtained by molecular replacement with the program PHASER (McCoy et al., 2007), using phases from the PDB_ID code 1ZN7 structure (Silva et al., 2008). The other structures were also solved by the molecular replacement method using our PRPP-Mg^{2+}-hAPRT structure as initial models. Complex structures were then refined with REFMAC5 (Murshudov et al., 1997) using the CCP4i software suite (Winn et al., 2011)_ENREF_54 and the building program COOT (Emsley et al., 2010).

Differential Scanning Fluorimetry Assays

The thermal stability of purified APRT protein was analyzed using a LightCycler 480 instrument (Roche) to image 384-wells simultaneously. The protein was diluted to 0.2 mg/ml in 20 mM Tris-HCl pH 7.4, 150 mM NaCl. This buffer maximized the fluorescence response. All the chemicals (ADE, PRPP, PPi, AMP) were used at the same concentrations in all the experiments (1 mM final concentration in 1 % DMSO). Optical foil was used to cover the PCR microplates (Roche). The plates (containing a total of 10 μL/well) were centrifuged, placed in the LightCycler apparatus and the temperature of protein solution gradually increased from 30 to 95°C at 0.01°C per second with 16 acquisitions per degree. The protein stability was assessed by measuring the fluorescence of a reporter dye, SYPRO orange (Invitrogen, Carlsbad, S6651), diluted 1000-fold as recommended by the manufacturer, which interacts specifically with the hydrophobic patches of the protein. Filters were adjusted to the optimal excitation and emission wavelengths for SYPRO Orange (Ex 465 / Em 580 nm). Each experiment was performed in triplicate in order to compute the mean value of the thermal melting profile (Tm) and its standard deviation.

In Vitro hAPRT Kinetic Analysis

In the forward reaction, human wild-type APRT and Tyr105Phe variant activities were determined by quantifying the amount of AMP produced using a spectroscopic assay identical to the one developped in J.V. Tuttle et al. (Tuttle and Krenitsky, 1980). Analyses were performed in 0.1 M Tris-HCl pH 7.5, 10 mM $MgCl_2$ (buffer D), or in the crystallization buffer 85 mM Tris pH=8.5, 5 mM $MgCl_2$, 170 mM NaOAc, 17% PEG4000 and 15% glycerol. The latter solution needed to be prepared freshly so as not to give a signal at 256 nm. The reaction mixture (200 μL final volume) was incubated at 23°C. When ADE was varied, 500 μM of PRPP were added to the mixture. When PRPP was varied, 50 μM of ADE were added to the mixture. The wild type protein concentration used was 200 nM and 600 nM respectively in buffer D and crystallization buffer. For the variant enzyme, the protein concentration used was 2 μM and 4 μM respectively in buffer D and crystallization buffer. The reaction started after the addition of the enzyme and was monitored at 256 nm, where the differential of the absorbance is maximum between AMP and ADE and equal to 2,100 $M^{-1}.cm^{-1}$ (Tuttle and Krenitsky, 1980). Inhibitory constant (K_i) of AMP versus PRPP were calculated using 0, 20 and 80 μM concentration of AMP in the reaction mixture. The

equilibration constant (K_{eq}) were calculated at equilibrium as [AMP][PPi]/[ADE][PRPP] while incubating equimolar concentration of ADE and PRPP and measuring the molar concentration of AMP formed (also equal to the concentration of PPi). The kinetic parameters were determined with the Michaelis-Menten equation using Origin 6.1 with a hyperbolic fit. For the reverse reaction, a coupled enzymatic reaction similar to the one described in Bashor et al. was used (Bashor et al., 2002). The reaction mixture (60 μL final volume) was incubated at 37°C. AMP, PPi and quinolinic acid (QA) were respectively added at 1.0, 0.5 and 0.5 mM final concentration. Human QPRT (ε = 26,900 $M^{-1}.cm^{-1}$) and hAPRT were then added at 25 and 10 μM, respectively. After a 30-minute incubation, the reaction was stopped by addition of 60 μL of 2M KCN. The nicotinic acid mononucleotide (NaMN) derivative was then monitored at 315 nM with an absorbance coefficient of 5,500 $M^{-1}.cm^{-1}$ (Colowick et al., 1951). All measurements were done in triplicates.

APRT Mutagenesis

A human wild-type *APRT* gene optimized for yeast expression was purchased from DNA2.0 (CA, USA). This gene, flanked by *Bgl*II and *Nsi*I restriction sites, was cloned into a pJ201 vector (DNA2.0) to give the p4489 plasmid. Mutant genes were obtained by PCR using p4489 as template and oligonucleotides 5'-CTATGGGCATCTTACTCACTTCTATATGGAAAGGCT GAACTTG-3' and 5'- CAAGTTCAGCCTTTCCATATAGAAGTGAGTAAGATGCCCATAG-3' for the E104L mutant and oligonucleotides 5'-GGGCATCTTACTCACTTGAATTTGGAAAGGCTGAACTTGAAATTC-3' and 5'-GAATTTCAAGTTCAGCCTTTCCAAATTCAAGTGA GTAAGATGCCC-3', for the Y105F mutant. Wild-type and mutated *APRT* genes were then cloned into a tetracycline-repressible vector pCM189 (*CEN*, *URA3*) (Gari et al., 1997) by transferring the *Bgl*II–*Nsi*I cassette from the pJ201 plasmid into pCM189 opened with *Bam*HI and *Pst*I, thus giving the p4521, p4911 and p4912 plasmids for wild-type, E104L and Y105F APRT, respectively.

Yeast Medium, Growth Tests and Metabolite Determinations

SD is a synthetic minimal medium which contains 5% ammonium sulfate, 0.17% yeast nitrogen base (BD-Bioscience), 2% glucose. SDcasaW is SD medium supplemented with 0.2% casamino acids (BD-Bioscience) and tryptophan (0.2 mM). When indicated, adenine (0.3 mM) or hypoxanthine (0.3 mM) were added in the SDcasaW medium and the resulting media was named SDcasaWA (+ adenine) or SDcasaWHx (+ hypoxanthine). A *MATα ade2 apt1 aah1 ura3* yeast strain (DS1-2B/1, the generous gift of Dr. R. Woods, University of Winnipeg, Winnipeg, MB, Canada) was transformed with plasmids to allow the expression of wild-type (p4521) and mutated (p4911 and p4912) versions of human APRT, or the cognate empty vector (pCM189). Transformants were selected on SDcasaWHx medium and were then used for a drop growth test as described previously (Saint-Marc et al., 2009). For the quantification of purines in yeast, transformants were grown exponentially at 30°C for 24 h in SDcasaWHx medium. Cells were rapidly harvested by filtration (Sartolon polyamid filters 0.45μ, Sartorius stedim Biotech, USA) and then incubated for 3 hours at 30°C in either the SDcasaWHx or the SDcasaWA medium. The extraction of the yeast metabolites was done as previously described (Ceschin et al., 2014) and the metabolite separation was performed on an ICS3000 Chromatography Station (Dionex, Sunnyvale, USA) using a Carbopac PA1 column (250 x 2 mm; Thermo Electron SAS) with a 50 to 800 mM acetate gradient in 50 mM NaOH as described in Ceballos-Picot et al. (Ceballos-Picot et al., 2015). Peaks were identified by their retention times and/or their UV spectral signatures as well as by co-injection with standards. The detection of the human APRT by western blotting was done on total yeast protein extracts, obtained from exponentially grown cells as described in Escusa et al. (Escusa et al., 2006), using anti-human APRT (Abcam, ab196558) and anti-actin (gracefully given by J.A. Cooper, Washington University School of Medicine, St Louis, MO, USA) antibodies.

QUANTIFICATION AND STATISTICAL ANALYSIS

Cellular adenine, AMP and ATP concentrations were determined from 3 independent metabolite extractions for each condition as described in the methods. Kinetic data are presented as mean values from three independent experiments and the kinetic parameters were determined from the Michaelis-Menten equation. Error bars in all figures show standard deviations.

DATA AND SOFTWARE AVAILABILITY

The atomic coordinates and structure factors for the PRPP-Mg^{2+}-, ADE-PRPP-Mg^{2+}- and AMP-bound $hAPRT^{wt}$ as well as the $hAPRT^{Y105F\text{-}14hours}$, $hAPRT^{Y105F\text{-}14days}$ and $hAPRT^{Y105F\text{-}30days}$ complexe structures, reported in this paper, are deposited in the RCSB Protein Data Bank (www.rcsb.org) under the accession codes 6FCH, 6FCI, 6FCL, 6FD4, 6FD5, 6FD6, respectively.